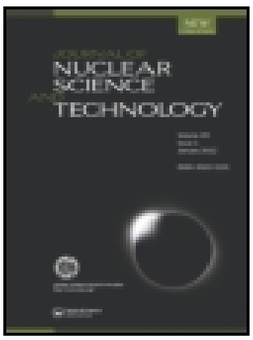

Journal of Nuclear Science and Technology

ISSN: (Print) (Online) Journal homepage: https://www.tandfonline.com/loi/tnst20

Benchmark experiment of large-angle scattering reaction cross section of iron at 14 MeV using two shadow bars – Comparison of experimental results with ENDF/B-VIII –

Atsuki Yamaguchi , Kazuki Fukui , Yuki Fujiwara , Shingo Tamaki , Sachie Kusaka , Fuminobu Sato & Isao Murata

To cite this article: Atsuki Yamaguchi , Kazuki Fukui , Yuki Fujiwara , Shingo Tamaki , Sachie Kusaka , Fuminobu Sato & Isao Murata (2020): Benchmark experiment of large-angle scattering reaction cross section of iron at 14 MeV using two shadow bars – Comparison of experimental results with ENDF/B-VIII –, Journal of Nuclear Science and Technology, DOI: 10.1080/00223131.2020.1804475

To link to this article: https://doi.org/10.1080/00223131.2020.1804475

Published online: 25 Aug 2020.

JOURNAL OF NUCLEAR SCIENCE AND TECHNOLOGY
https://doi.org/10.1080/00223131.2020.1804475

ARTICLE

OPEN ACCESS Check for updates

Benchmark experiment of large-angle scattering reaction cross section of iron at 14 MeV using two shadow bars – Comparison of experimental results with ENDF/B-VIII –

Atsuki Yamaguchi, Kazuki Fukui, Yuki Fujiwara, Shingo Tamaki, Sachie Kusaka, Fuminobu Sato and Isao Murata

Graduate School of Engineering, Osaka University, Osaka, Japan

ABSTRACT

It is important to perform neutron transport simulations with accurate nuclear data in the neutronics design of a fusion reactor. However, absolute values of large-angle scattering cross sections vary among nuclear data libraries even for well-examined nuclide of iron. Benchmark experiments focusing on large-angle scattering cross sections were thus performed to confirm the correctness of nuclear data libraries. The series benchmark experiments were performed at a DT neutron source facility, OKTAVIAN of Osaka University, Japan, by the unique experimental system established by the authors' group, which can extract only the contribution of large-angle scattering reactions. This system consists of two shadow bars, target plate (iron), and neutron detector (niobium). Two types of shadow bars were used and four irradiations were conducted for one experiment, so that contribution of room-return neutrons was effectively removed and only large-angle scattering neutrons were extracted from the measured four Nb reaction rates. The obtained experimental results were compared with calculations for five nuclear data libraries including JENDL-4.0, JEFF.-3.3, FENDL-3.1, ENDF/B- VII, and recently released ENDF/B-VIII. It was found from the comparison that ENDF/B-VIII showed the best result, though ENDF/B-VII showed overestimation and others are in large underestimation at 14 MeV.

ARTICLE HISTORY
Received 10 December 2019
Accepted 29 July 2020

KEYWORDS
Large-angle scattering; cross section; fusion reactor; nuclear data library; OKTAVIAN; 14 MeV; ENDF/B-VIII; JENDL-4.0; shadow bar

1. Introduction

It is important to perform simulations with accurate nuclear data in the neutronics design of a fusion reactor. Much efforts were given so far to benchmark the nuclear data. However, absolute values of large-angle scattering cross sections still vary among nuclear data libraries as shown in Figure 1. This is the case of iron, which is the most important element among fusion structural materials. Commonly this kind of cross-section behavior is seen for higher energy neutrons like DT neutron of 14 MeV. Practically, the angular differential cross section changes drastically as a function of scattering angle and the value is very small in backward angles. Ohnishi et al. reported however that though the absolute value was very small, the large-angle scattering cross section played an important role especially for gap-streaming calculations in fusion reactor [1]. Previously, there were measurements of double differential cross sections of secondary neutrons at 14 MeV [2], in which the angular differential cross sections were included [3]. However, such measurements are technically difficult, and in addition, there were no experimental approaches so far to directly measure and benchmark back-scattering neutrons because of the small cross sections as in Figure 1. In the present study, benchmark experiments were performed using an experimental system proposed by the authors' group [4] to examine large-angle scattering reaction cross sections. By this experimental technique, we can extract only large-angle scattering neutrons with a detection foil of niobium. We compare experimental results with simulations for several nuclear data libraries including newly released ENDF/B-VIII.

2. Experimental system

Figure 2 shows a conceptual experimental system to extract the contribution of large-angle scattering neutrons. The system design and preliminary experimental results were reported in Ref [4]. This experimental system consists of a DT neutron source, iron shadow bar, iron target plate, and neutron detector. The shadow bar is set up to suppress the direct incidence of 14 MeV neutrons to the detection foil, while the incident neutrons can enter the target plate directly. The incident neutrons to the target plate have at most one-time scattering, if the thickness of the target plate is appropriately thin. It means if the scattering is forward, the neutrons can go through the target plate, and if it is back-scattering, the neutrons can enter the detection foil. The foil can thus detect only large-angle-scattering neutrons from the target plate. However, we have to

CONTACT Isao Murata murata@see.eng.osaka-u.ac.jp Division of Sustainable Energy and Environmental Engineering, Graduate School of Engineering, Osaka University, Yamada-oka 2-1, Suita, Osaka, 565-0871, Japan

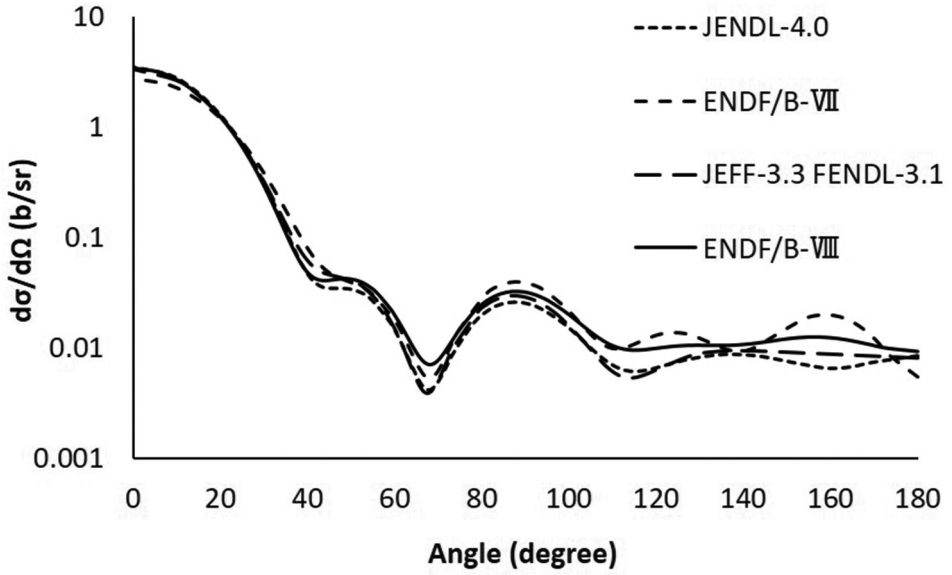

Figure 1. Angular distribution of neutron elastic scattering cross section of ^{56}Fe at 14 MeV [5–9].

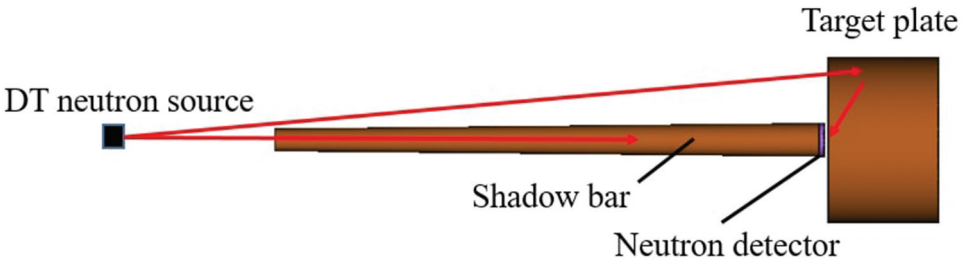

Figure 2. Conceptual experimental system to measure large-angle scattering neutrons.

consider troublesome room-return neutrons, because the experimental system is placed in a small irradiation room of ~4 × 4 × 4 m^3. The irradiation room is heavily shielded with 1~2 m thick walls made of ordinary concrete, the composition of which is oxygen (50%), silicon (32%), calcium (8%), aluminum (5%), sodium (2%), potassium (2%), and other impurity elements.

Two types of shadow bars (S1 and S2) with different shapes are used as shown in Figure 3. If the experimental system is not surrounded by a wall, large-angle

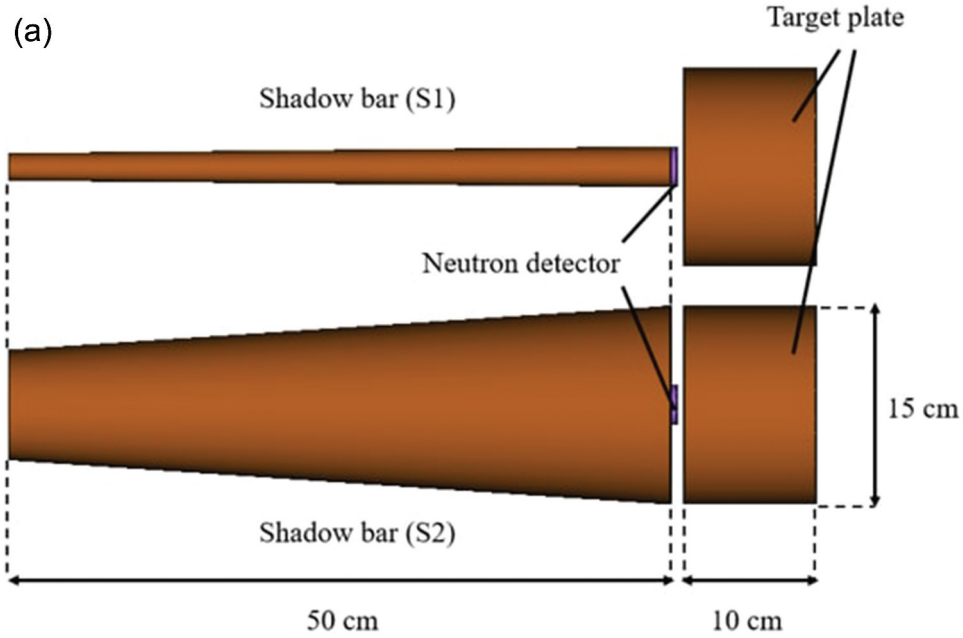

Figure 3. Experimental system arrangements with a narrow shadow bar (S1) and thick shadow bar (S2). (a) Experimental system arrangements. (b) Shadow bars.

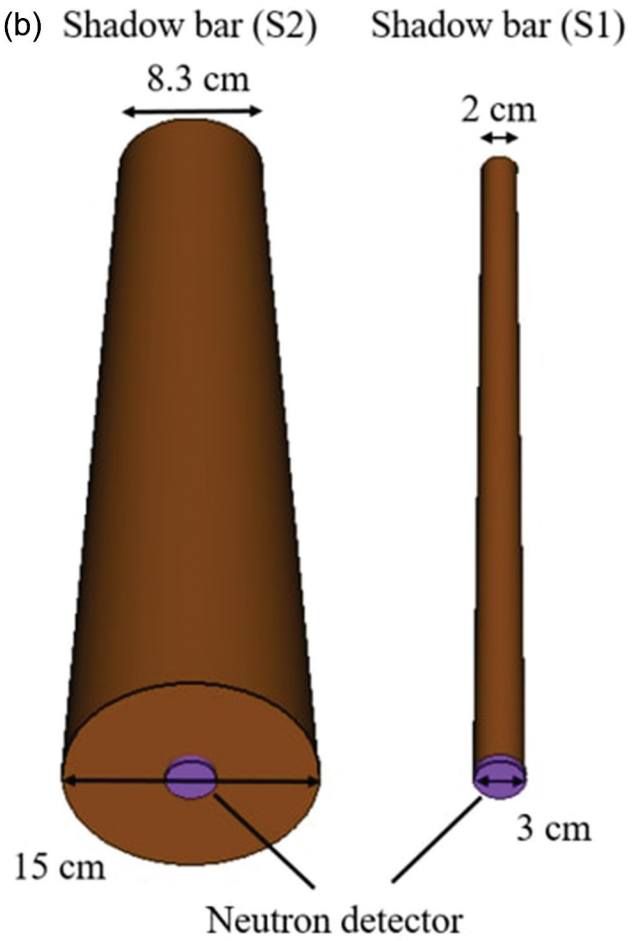

Figure 3. (Continued).

scattering neutrons can be measured by carrying out two types of experiments, target-in with S1 and target-out with S1. However, in practical experiments, we have to consider room-return neutrons because there exists a wall in the experimental room. To cope with this situation, two types of shadow bars (S1 and S2) are used. It means, we carry out four experiments in total, i.e. target-in with S1, target-out with S1, target-in with S2 and target-out with S2. The reason to employ this experimental procedure is as follows. With shadow bar S1, carrying out two experiments, target-in and -out, and taking the difference between the two results, the contributions of large-angle scattering neutrons and room-return neutrons except directly incident neutrons to the foil can be measured. On the other hand, with shadow bar S2, carrying out the other two experiments, target-in and -out, and via similar process, the contribution of room-return neutrons except directly incident neutrons to the foil can be measured. By subtracting the above result with S2 from the one with S1, the contribution of large-angle scattering neutrons can be extracted. More details are given in Section 3.2 to understand the relation of the actual neutron transport path and the neutron contribution to niobium activity in each experimental case.

The shadow bar material is made of iron because the macroscopic cross section at 14 MeV is large to attenuate the 14 MeV neutrons. The shadow bars are circular-truncated cones and the dimensions of the shadow bar S1 are 50 cm in length, 2 cm in upper diameter, and 3 cm in bottom diameter and those of S2 are 50 cm in length, 8.3 cm in upper diameter, and 15 cm in bottom diameter. These dimensions were optimized by parameter survey calculations by MCNP-5 [4]. The distance between the DT neutron source and the upper base of the shadow bar was also optimized as 55 cm. This distance deeply depends on the shape of the shadow bar.

The dimensions of the iron target plate are 15 cm in diameter and 10 cm in thickness. By making the target plate appropriately thin, i.e. around 2 mean free path (MFP), we can reduce the number of forward scattering reactions inside the target plate and simultaneously make the contribution of the large-angle scattering reaction dominant. Of course, if the thickness is thinner than 2 MFP, the ratio of large-angle scattering neutrons will be improved. However, the absolute number of large-angle scattering neutrons goes down, and as a result, the amount of foil activation decreases. This value (2 MFP) was finally

determined so as to complete the whole measurement within one week.

For the detection foil, we employed niobium, the size of which is 5 mm in thickness and 3 cm in diameter. The diameter is the same as the bottom diameter of the shadow bar S1. The reason why we chose niobium is in the following. Scattering neutron energy in the laboratory system, E_n, can be expressed by the next equation for scattering angles, θ, simply derived from kinematics of elastic scattering reaction.

$$E_n = \frac{E_L}{2} \cdot (1 + \alpha + (1 - \alpha) \cdot cos\theta) \quad (1)$$

where E_L is the incident neutron energy, $\alpha = \frac{(A-1)^2}{(A+1)^2}$ and A is the mass ratio of the target material to neutron.

Figure 4 shows the calculation results for various nuclides by this equation. In Figure 5, the activation cross section of ^{93}Nb(n,2n)^{92m}Nb reaction is described, which is cited from JENDL/AD-2017 [10]. This reaction has the following features: The reaction

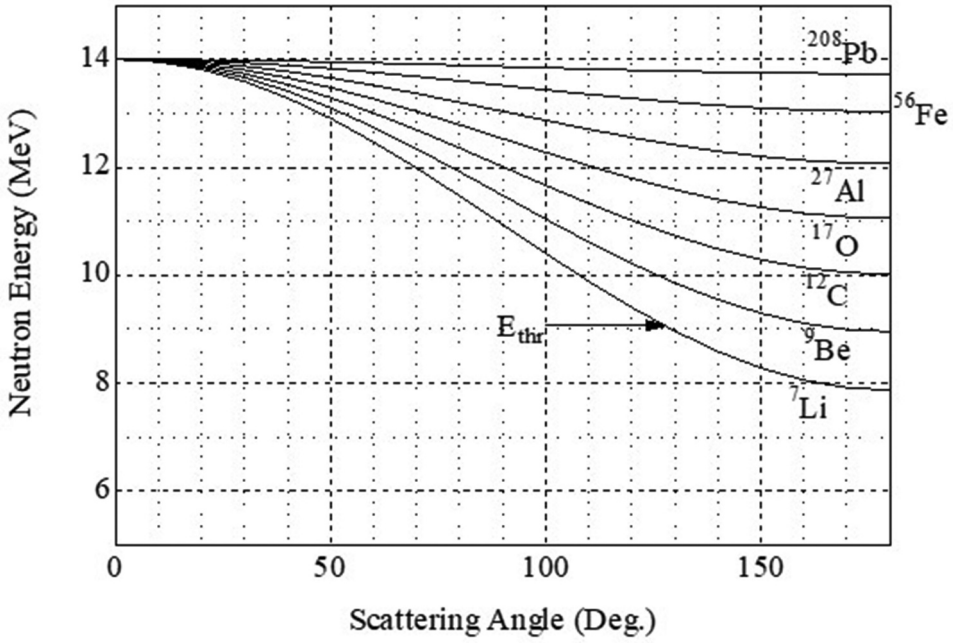

Figure 4. Neutron energy after elastic scattering for various nuclides as a function of scattering angle for incident neutron energy of 14 MeV.

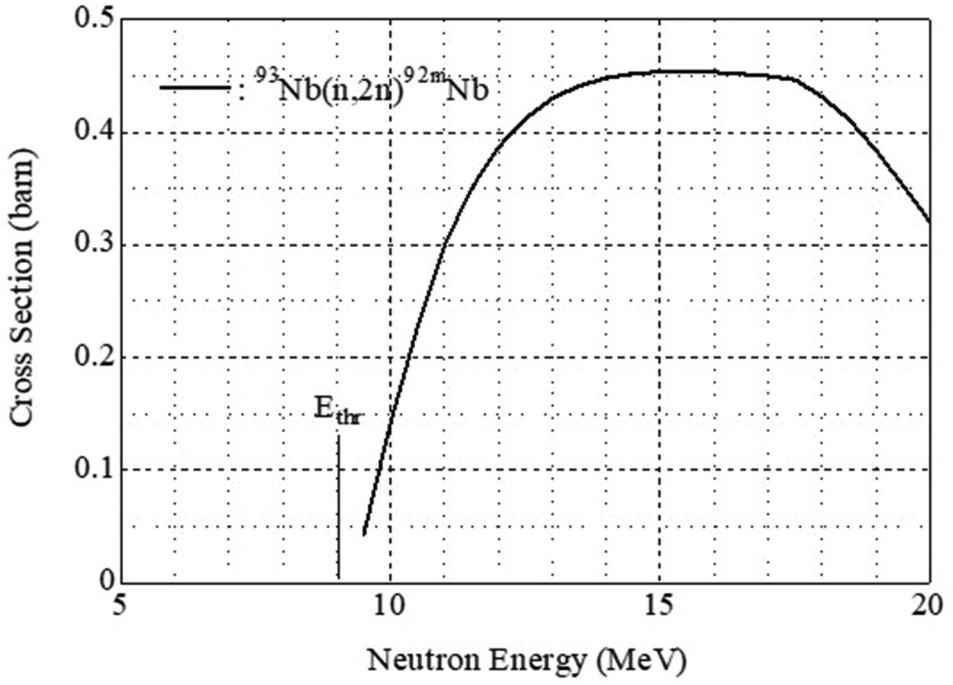

Figure 5. ^{93}Nb(n,2n)^{92m}Nb reaction cross section.

has a high threshold energy of 9.1 MeV, the cross-section value sharply increases for neutron energy, and it becomes a flat value at around 15 MeV. From Figure 4, for nuclides heavier than ^{27}Al, the energy even for 180-degree scattering is higher than 12 MeV, and in this case, from Figure 5 the activation cross-section value of niobium is found to be enough high, i.e. ~0.4 barn. These facts indicate that the niobium foil can firmly count large-angle scattering neutrons emitted from the target plate made of medium-heavy or heavier atoms.

3. Numerical simulation

This chapter details how large-angle scattering neutrons can be extracted using the experimental procedure described in Chapter 2. First, the calculation method to treat the four experimental configurations accurately using MCNP-5 will be described. Then, it explains how we can estimate the contribution of large-angle scattering neutrons by considering all of the possible neutron transport paths in the four experiments.

3.1. Simulation with MCNP5

Four numerical experiments were carried out with MCNP5 for each shadow bar, S1 and S2, and with and without the target plate for new nuclear data libraries, ENDF/B-VIII, FENDL-3.1, and JEFF-3.3, in addition to the previous results for ENDF/B-VII and JENDL-4.0 [4]. F4 tally was used to calculate the reaction rate of niobium foil. Seven paths of neutrons (①~⑦) were taken into account as shown in Figure 6(a,b) to extract the contribution of large-angle scattering neutrons. To separate these seven contributions, cell flagging was employed in MCNP5 calculations, i.e. flags were set to 'Wall,' 'Shadow bar,' and 'Target plate' in Figure 6. Relation of the paths and the flags is summarized in Table 1. For the three flags, we need to consider seven paths calculated by $_3C_1 + _3C_2 + _3C_3$. As shown in the figure, path ① is that neutrons just pass through the shadow bar to reach the Nb foil, in path ②, neutrons are scattered in the shadow bar and reflected in the target plate to reach the foil, in path ③, neutrons are reflected only in the target plate to reach the foil, in path ④, after reflected in the wall, neutrons reach the foil via the shadow bar, in path ⑤, after reflected in the wall, neutrons reach the foil via the target plate, in path ⑥, neutrons are reflected only in the wall to reach the foil, and in path ⑦, neutrons pass through all the three flagged cells in one history. The large-angle scattering neutrons are neutrons transporting in path ③. We need to determine the contribution of neutron, ③, by the four experiments.

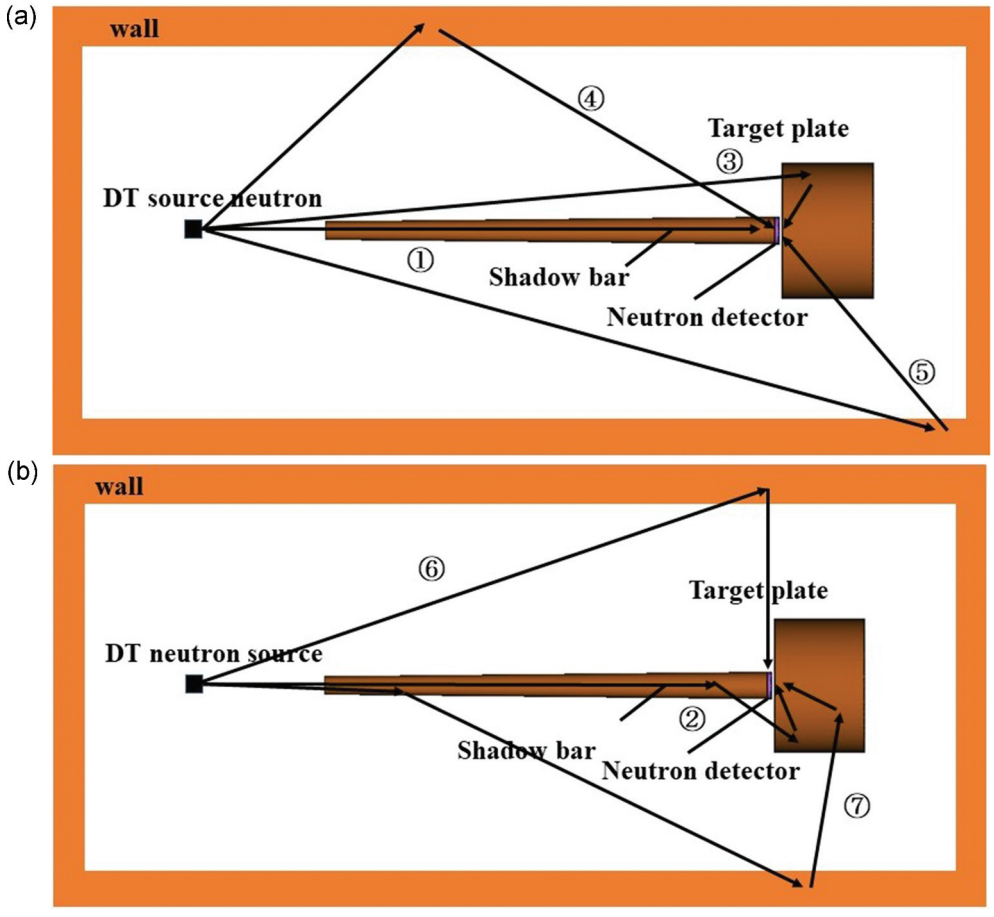

Figure 6. Separation of the paths of neutrons. (a) Paths ①, ③, ④, ⑤. (b) Paths ②, ⑥, ⑦.

Table 1. Relation of six paths and three flags.

		Flag status (○: On, —: Off)						
Flagged cell	Wall	○	—	—	○	○	—	○
	Shadow bar	—	○	—	○	—	○	○
	Target plate	—	—	○	—	○	○	○
Transport path No. in Figure 6		⑥	①	③	④	⑤	②	⑦

3.2. Extraction of large-angle scattering neutron

Table 2 shows the calculation summary in the case of using ENDF/B-VIII. Suffixes 'it' and 'nt' mean experiments with and without the target plate, respectively. The numbers ①~⑦ correspond to the separated neutron paths shown in Figure 6. It can instantly be recognized that contribution ③ is included in the foil of S1it. However, other path contributions are also contained in the calculation. The other contributions can be deduced and removed because the contributions are contained also in the other three foils. Finally, contribution of large-angle scattering neutrons (③) can be derived by the four Nb reaction rates with the next equation.

$$\text{Contribution ③} = (\text{S1it}) - (\text{S2it}) - ((\text{S1nt}) - (\text{S2nt})) \tag{2}$$

The reason is in the following: Most contributions for paths are to be a pair and compensated with each other by the above equation. For instance, for ①, ④, and ⑥ pairs are made for cases, S1it and S1nt, and S2it and S2 nt. Practically, in case of ①, S1it and S1nt are 0.01 (10^{-9} reaction/source neutron/cm^3) and S2it and S2 nt are 0.1 (10^{-9} reaction/source neutron/cm^3), and as can be understood in Figure 6(a), the contribution ① is expected to change due to the shadow bar size, however, not change irrespective of the existence of the target sample, because ① is the path that only passes through the shadow bar. It means that the contributions for S1it and S1nt become the same and those of S2it and S2 nt become the same. We can understand the trend of contributions ④ and ⑥ similar to ①. And for ⑤, similarly, contributions of S1it and S2it are compensated and S1nt and S2nt are compensated as well. For residual contributions ② and ⑦, ② remains uncompensated while for ⑦ compensation is weakly observed. The reason for the weak compensation of ⑦ is that in this case neutrons pass through all the three flagged cells as shown in Table 1. In any case, fortunately, these contributions are enough small compared to that of large-angle scattering neutrons in path ③. We recognize that contribution ② becomes the estimation error.

Table 2. Reaction rate of ^{93}Nb(n,2n)^{92m}Nb reaction rate for each path in each experiment calculated using ENDF/B-VIII. (unit: 10^{-9} reaction/source neutron/cm^3).

	S1it	S2it	S1nt	S2nt	S1it − S2it − (S1nt − S2nt)
①	0.01	0.10	0.01	0.10	0
②	0.13	0.00	0	0	0.13
③	4.98	0	0	0	4.98
④	1.00	0.59	1.00	0.59	0
⑤	1.05	1.05	3.02	2.95	−0.06
⑥	0.74	0.23	0.74	0.23	0
⑦	0.02	0.05	0.02	0.07	0.01
Sum	7.94	2.02	4.79	3.93	5.06

4. Experimental result and discussion

We carried out four experiments, S1it, S1nt, S2it, and S2nt, at OKTAVIAN facility in Osaka University. Irradiation time in each experiment was 15 hours. The 14 MeV neutron source intensity is 5.0×10^9 ~ 1.0×10^{10} n/s. The radioactive Nb foils were measured by an HPGe detector. Table 3 shows ^{93}Nb(n,2n)^{92m}Nb reaction rates for experimental and simulation results. Simulation results were obtained using ENDF/B- VII, ENDF/B- VIII, JENDL-4.0, FENDL-3.1, and JEFF-3.3. Table 3 indicates that the recently released ENDF/B-VIII shows the best result among the libraries. The discrepancy is just 7% underestimation. Overestimation (16%) is observed for ENDF/B-VII, and underestimation (~17%) is seen for JENDL-4.0, FENDL-3.1, and JEFF-3.3. The tendency of these results is found to excellently be consistent with the cross sections shown in Figure 1, i.e. the angular differential cross section of ENDF/B-VII is always larger than ENDF/B-VIII in backward angles. Also, the other cross sections in Figure 1 are clearly smaller compared to the ones of ENDFs for angles larger than 90 degrees. The correct value may thus exist in between ENDF/B-VII and ENDF/B-VIII. From the present result of Table 3 and the trend of Figure 1, it can be confirmed that the present technique can successfully extract the cross-section difference numerically in backward scattering angles and can perform a direct comparison of numerical and experimental results using niobium activities in order integrally to benchmark backward angle scattering cross section.

It is additionally noted that the angle distribution of neutron elastic scattering cross section of ^{56}Fe for FENDL-3.1 is the same as that for JEFF-3.3, however, the results for them are slightly different as in Table 3. This is because evaluations of the angular distribution of neutron elastic scattering cross section of ^{54}Fe and ^{57}Fe are different for FENDL-3.1 and JEFF-3.3.

This technique would be a powerful tool to directly benchmark large-angle scattering cross section and can be applied to tests of various scattering reaction cross sections for fusion structural materials in the future.

5. Conclusion

Benchmark experiments of large-angle scattering reaction cross section of iron were performed, and the results were compared with calculations for five

Table 3. Measured four ^{93}Nb(n,2n)^{92m}Nb reaction rates and large-angle scattering neutron contribution (③) compared to numerical simulation results for five nuclear data libraries. (unit: 10^{-9} reaction/source neutron/cm^3).

	S1it	S2it	S1nt	S2nt	S1it − S2it − (S1nt − S2nt)
Experimental result*	8.31 ± 0.06	1.68 ± 0.06	5.01 ± 0.14	3.83 ± 0.03	5.45 ± 0.17
ENDF/B-Ⅶ	9.32	2.06	4.80	3.91	6.37
ENDF/B-Ⅷ	7.94	2.02	4.79	3.93	5.06
JENDL-4.0	7.00	1.98	4.84	3.93	4.11
FENDL-3.1	6.99	2.09	4.83	3.97	4.04
JEFF-3.3	6.85	2.08	4.82	3.98	3.92

* The experimental errors are estimated by the count number of each measurement of the foil and the error of the contribution ③ was estimated by propagating the statistical errors of four experimental results by Equation (2).

nuclear data libraries including recently released ENDF/B-VIII. It was found that ENDF/B-VIII showed the best result at 14 MeV, practically the discrepancy of experiment and simulation is just 7% for the niobium reaction rate induced only by back-scattering neutrons. We recognized that the present technique was successful because the tendency of Table 3 was excellently consistent with the cross-section values for backward angles in Figure 1. In the next step, we will perform benchmark experiments on structural material elements of fusion reactor other than iron, like lead, silicon, tungsten, and so on, to verify their large-angle scattering cross sections.

Disclosure statement

No potential conflict of interest was reported by the authors.

References

[1] Ohnishi S, Kondo K, Azuma T, et al. New integral experiments for large-angle scattering cross section data benchmarking with DT neutron beam at JAEA/FNS. Fusion Eng Des. 2012;87:695–699.

[2] Takahashi A, Ichimura E, Sasaki Y, et al. Measurements of double differential neutron emission cross sections for incident neutrons of 14 MeV. J Nucl Sci Technol. 1988;25:215–232. Takahashi A. Measurements of double differential cross sections at OKTAVIAN. *J. Nucl. Sci. Technol.*, 1989; 26: 15-20.

[3] Takahashi A, Ichimura E, Sasaki Y, et al. Double and single differential neutron emission cross sections at 14.1 MeV. OKTAVIAN report; 1987. Vol. 1. A-87-03 385. Takahashi A, Gotoh M, Sasaki Y, Sugimoto H. Double and Single Differential Neutron Emission Cross Sections at 14.1 MeV: Vol. 2. OKTAVIAN Report 1992; A-92-01 577.

[4] Hayashi N, Ohnishi S, Fujiwara Y, et al. Optimization of experimental system design for benchmarking of large-angle scattering reaction cross section at 14MeV using two shadow bars. Plasma Fusion Res. 2018;13 (2405002):4.

[5] Shibata K, Iwamoto O, Nakagawa T, et al. JENDL-4.0: a new library for nuclear science and engineering. J Nucl Sci Technol. 2011;48:1–30.

[6] Chadwick MB, Herman M, Obložinský P, et al. ENDF/B-VII.0: next generation evaluated nuclear data for nuclear science and technology. Nucl Data Sheets. 2006;102:2931–3060.

[7] JEFF-3.3. France: nuclear energy agency. 2018. [cited 2019 Aug 1]. Available from: https://www.oecd-nea.org/dbdata/jeff/jeff33/index.html

[8] FENDL-3.1. Austria: NDS. IAEA - International Atomic Energy Agency; 2018 Jan 24. [cited 2019 Aug 1]. Available from: https://www-nds.iaea.org/fendl/

[9] Brown DA, Chadwick MB, Capote R, et al. ENDF/B-VIII.0: the 8th major release of the nuclear reaction data library with CIELO-project cross sections, new standards and thermal scattering data. Nucl Data Sheets. 2018;148:1–142.

[10]. Shibata K, Iwamoto N, Kunieda S, et al. Activation cross-section file for decommissioning of LWRs. JAEA-Conf 2016-004. 2017;47–52.